

E-field Control of the RKKY Interaction in FeCoB/Ru/FeCoB/PMN-PT (011) Multiferroic Heterostructures

Xinjun Wang, Qu Yang, Lei Wang, Ziyao Zhou,* Tai Min, Ming Liu,* and Nian X. Sun*


E-field control of antiferromagnetic (AFM) orders is promising for the realization of fast, compact, and energy-efficient AFM applications. However, as the AFM spins are strongly pinned, the E-field control process is mainly based on the exchange bias regulation that usually confines at a low temperature. Here, a new magnetoelectric (ME) coupling mechanism for the modulation of AFM orders at room temperature is explored. Based on the FeCoB/Ru/FeCoB/(011) $\text{Pb}(\text{Mg}_{1/3}\text{Nb}_{2/3})\text{O}_3\text{-PbTiO}_3$ (PMN-PT) synthetic antiferromagnetic (SAF) heterostructures, the external E-field generates relative magnetization switching in the two ferromagnetic (FM) layers, leading the Ruderman–Kittel–Kasuya–Yosida (RKKY) interaction tuning. This voltage-induced switching behavior can be repeated in a stable and reversible manner for various SAFs, which is a key challenge in the E-field control of AFM coupling and is not resolved yet. The voltage-induced RKKY interaction changes by analyzing the dynamic optical and acoustic modes is quantified, and with first-principles calculations, it is found that the distortion of the Fermi surface by the lattice reconstruction is the key of the relative magnetization switching and RKKY interaction modulation. This voltage control of the RKKY interaction in ME heterostructures provides an easy way to achieve the next generation of AFM/FM spintronic applications.

Antiferromagnetic (AFM) spintronics has aroused extensive research interest due to the high magnetic field (H-field) stability^[1,2] and ultrafast operation speed,^[3] making it a great candidate for next generation of spintronic applications. Despite its

X. Wang, Prof. N. X. Sun
Department of Electrical and Computer Engineering
Northeastern University
Boston, MA 02115, USA
E-mail: n.sun@northeastern.edu

Q. Yang, Prof. Z. Zhou, Prof. M. Liu
Electronic Materials Research Laboratory
Key Laboratory of the Ministry of Education
State Key Laboratory for Mechanical Behavior of Materials
Xian Jiaotong University
Xi'an, Shaanxi 710049, China
E-mail: ziyaozhou@xjtu.edu.cn; mingliu@xjtu.edu.cn

Dr. L. Wang, Prof. T. Min
Center for Spintronics and Quantum System
State Key Laboratory for Mechanical Behavior of Materials
School of Materials Science and Engineering
Xi'an Jiaotong University
Xi'an, Shaanxi 710049, China

 The ORCID identification number(s) for the author(s) of this article can be found under <https://doi.org/10.1002/adma.201803612>.

DOI: 10.1002/adma.201803612

merits, the control of AFM orders remains challenging since the antiparallel AFM spins are extremely insensitive to external H-field. Existing researches mainly focus on the spin-polarized current control method,^[1,4] in which the large current density problem may hinder its practical application. As an alternative, electric field (E-field) control of antiferromagnetism through magnetoelectric (ME) coupling has aroused wide research interests in the last decade because it is a promising way to realize the fast, compact, and energy-efficient spintronic devices. Due to the invisible AFM spins, the E-field control mainly relies on the indirect measurements like exchange bias.^[5,6] Nevertheless, the pinning effect at AFM–ferromagnetic (FM) interface is usually too strong to operate at room temperature.^[6]

To overcome these difficulties, the synthetic antiferromagnetic (SAF) multilayer with an FM/nonmagnetic (NM)/FM sandwich structure is considered as an easier way to manipulate the AFM orders.^[2,7,8] In this SAF multilayer structure with Ruderman–Kittel–Kasuya–Yosida (RKKY) interaction, the top and bottom FM layers are coupled indirectly through the itinerant electrons in the NM middle layer.^[8–10] The interlayer exchange coupling (IEC) of the two FM layers can be parallelly or antiparallelly coupled,^[11,12] corresponding to the typical “0” or “1” state for information storage. The rapid growth of giant resistance (GMR) technology has inspired enormous research efforts for the RKKY interaction study in FM/NM/FM sandwich heterostructures.^[13,14] Significant progress has been achieved in the voltage controllable SAFs via ionic liquid/gel gating method.^[12,15] Nevertheless, this gating method suffers from a recovery problem because of the limited electrochemical reaction. E-field control of RKKY interaction in a clean and fully reversible manner, which is at a premium for the development of novel spintronic devices, remains unachieved.

In this work, we demonstrated a new approach toward E-field controllable AFM–FM coupling switching at room temperature based on the FeCoB/Ru/FeCoB/(011) $\text{Pb}(\text{Mg}_{1/3}\text{Nb}_{2/3})\text{O}_3\text{-PbTiO}_3$ (PMN-PT) multiferroic heterostructures. A series of SAFs with different Ru thicknesses (t_{Ru}) were fabricated, and a clear Ru thickness dependence of RKKY interaction strength was revealed. We studied the E-field control of IEC systematically via both the vibrating sample magnetometer (VSM) and the ferromagnetic resonance (FMR) measurement. At different

temperature based on the FeCoB/Ru/FeCoB/(011) $\text{Pb}(\text{Mg}_{1/3}\text{Nb}_{2/3})\text{O}_3\text{-PbTiO}_3$ (PMN-PT) multiferroic heterostructures. A series of SAFs with different Ru thicknesses (t_{Ru}) were fabricated, and a clear Ru thickness dependence of RKKY interaction strength was revealed. We studied the E-field control of IEC systematically via both the vibrating sample magnetometer (VSM) and the ferromagnetic resonance (FMR) measurement. At different

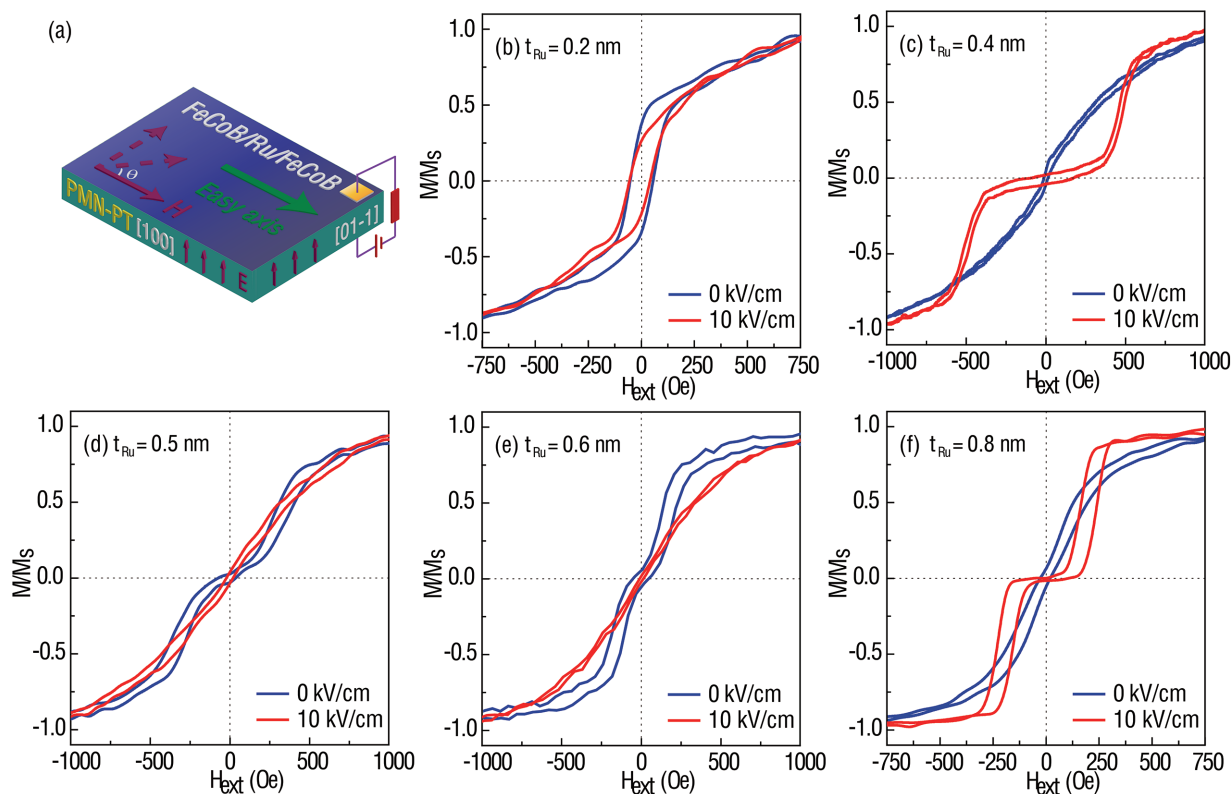


Figure 1. E-field control of RKKY interaction along [100] direction. a) Schematic for E-field controllable FeCoB/Ru/FeCoB/PMN-PT SAFs. b–f) Corresponding magnetic hysteresis loops switching at $t_{\text{Ru}} = 0.2, 0.4, 0.5, 0.6,$ and 0.8 nm, respectively.

Ru thicknesses, double/single loops switched electrically in a reversible and stable manner. Along the [100] direction of $t_{\text{Ru}} = 0.4$ nm SAF, the initial single magnetic hysteresis ($M-H$) loop switches electrically to double $M-H$, while the double $M-H$ loop of $t_{\text{Ru}} = 0.6$ nm SAF becomes single $M-H$ loop. There was angular anisotropy and the situation is quite different along the [01-1] direction, but stable E-field-induced AFM-FM coupling switches were realized at both orientations. This was the first time that researchers obtained the reversibility in the voltage regulation of AFM order without any sacrifice of the control effect, which can be important for the next generation of AFM-FM switchable spintronics with high energy efficiency. We related the voltage controlled RKKY exchange coupling to the E-field-induced lattice deformation, and the corresponding changes of the IEC can be understood by the distortion of the Fermi surface by a relevant first-principles calculation.

To study the E-field control of RKKY interactions, a series of $\text{Fe}_{60}\text{Co}_{20}\text{B}_{20}$ (15 nm)/Ru (x nm)/ $\text{Fe}_{60}\text{Co}_{20}\text{B}_{20}$ (15 nm) SAFs with different t_{Ru} were deposited onto PMN-PT (011) piezoelectric substrates. In this SAF sandwich structure, two FM layers are separated by an NM layer,^[10,12,13] and they have indirect interaction through IEC.^[8] According to the RKKY theory,^[10,12] the measured $M-H$ loops of SAF can reveal a clear Ru thickness because the IEC is an oscillatory function of the spacer thickness, which is continuous with our experimental results. As shown in **Figure 1**, when t_{Ru} increases from 0.2 to 0.8 nm, the hysteresis loop varies from single (0.2, 0.4 nm) to double (0.5, 0.6 nm) and then back to the single (0.8 nm) mode. With

an applied voltage across the PMN-PT thickness direction, the strain effect generates lattice distortion and then affects the IEC as well as the coupling modes. Due to the film magnetic anisotropy and the substrate deformation difference along various directions, there are different RKKY interactions and voltage responses. For the [100] direction, using the measurement method shown in **Figure 1a**, the RKKY interactions can be tuned electrically as displayed in **Figure 1b–f**. When $t_{\text{Ru}} = 0.2$ nm, the FM coupling is strong and the magnetization of the two FeCoB layer couples firmly in parallel. With the applied E-field of 10 kV cm^{-1} , the FM coupling strength is changed, but the RKKY mode is not switched (**Figure 1b**). In contrast, as t_{Ru} increases to 0.4 nm, the $M-H$ loop changes from initial single-loop into a double-loop pattern under an E-field. As shown in **Figure 1c**, E-field weakens the FM coupling strength, leading to a double $M-H$ loop. Detailed transition process under an increasing E-field can be found in **Figure S1** in the Supporting Information for the single \leftrightarrow double loop switching. The opposite trend can also be realized by electrically transforming the double loop into a single one (**Figure 1d,f**). As t_{Ru} keeps increasing to 0.8 nm, the IEC comes to the second single-loop state interval with decreasing strength, and the external E-field manages to switch the single mode into the double mode. Fascinating phenomena can also be obtained during the ionic liquid gating of RKKY interaction, but this voltage control method can hardly have both the control effect and the perfect reversibility due to the limited chemical reaction.^[12] Therefore, the E-field control of RKKY interaction in a

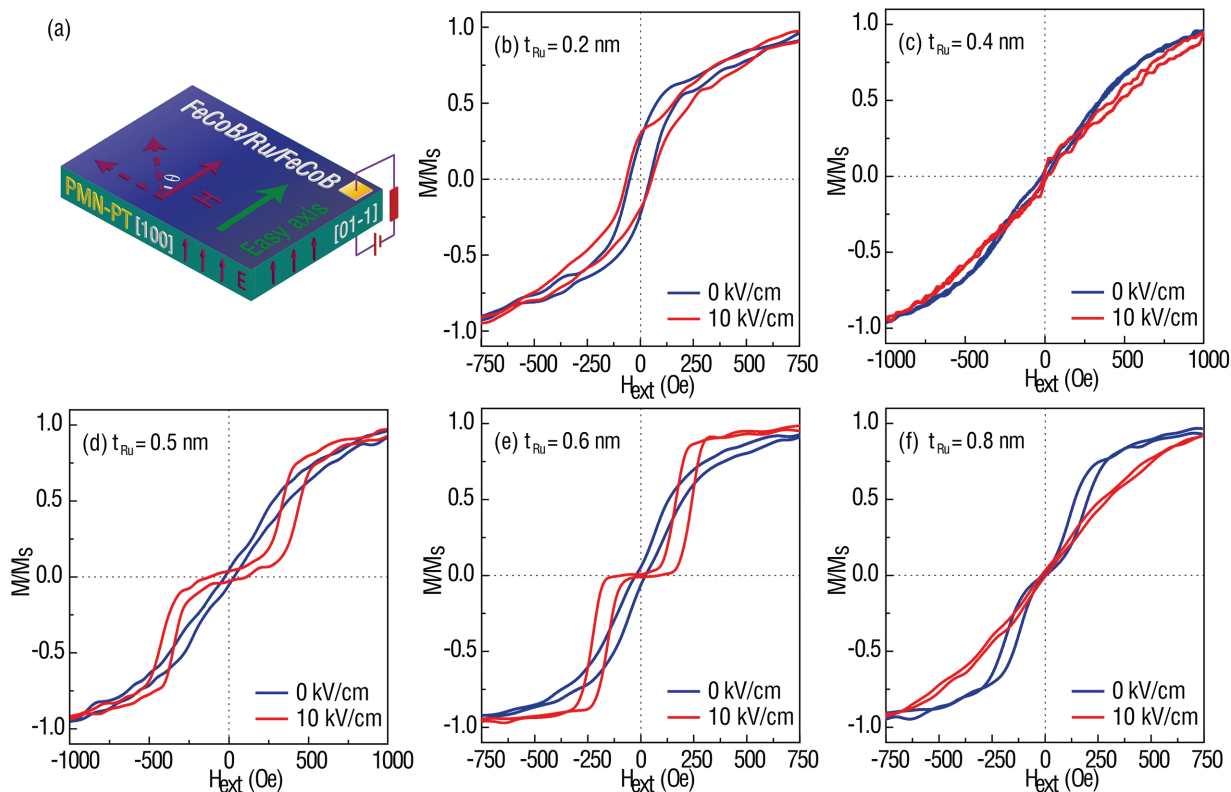


Figure 2. E-field control of RKKY interaction along [01–1] direction. a) The voltage control schematic for the case of the H-field along [01–1] direction. b–f) The regulation results for various Ru thickness. The loops clearly indicate a single \leftrightarrow double loop-switching behavior, which corresponds to the FM–AFM transition.

reversible manner is a significant improvement for the AFM coupling regulation.

Figure 2 displays the E-field controllable RKKY interaction of [01–1] direction. Because of the in-plane magnetic anisotropy and the substrate deformation difference along various directions, there are different IECs. Nevertheless, similar thickness dependence (i.e., alternate change of FM–AFM–FM) can also be observed, and the switching between AFM \leftrightarrow FM couplings is also realized. We will discuss the voltage control of RKKY interaction in detail based on **Figure 3**. The chosen sample for discussion is the 0.4 nm SAF, and the typical switching of M – H loops along [100] direction is shown in **Figure 3a**. At external H-field of 360 Oe, the relative magnetization angle in the two FM layers reverses remarkably, which can be illustrated by the arrows. By applying voltage pulses of opposite polarity with an amplitude of 10 kV cm^{-1} and duration of 100 ms, we studied corresponding magnetization switching as shown in **Figure 3b**. The magnetic moment switches stably between $-0.63 M_s$ and $+0.63 M_s$ with an H-field (360 Oe) assistance, confirming a non-volatile, reversible switching behavior. The 100 ms voltage pulse was utilized to guarantee a complete magnetization switching, not for the consideration of ultrafast response speed; more detail work can be carried out to study the ultrafast response dynamics tuned by E-field.

The E-field switching of AFM \leftrightarrow FM modes in the SAF heterostructures originates from the strain/stress effect of the piezoelectric substrate. As shown in **Figure 3c**, the external E-field

across the thickness direction leads to a lattice distortion in the SAF sample, giving the Fermi surface a distortion (discussed later). A similar phenomenon can also be found in [01–1] direction as shown in **Figure 2**. Polarization–electric (P – E) loop and E-field dependence of strain effect for the (011) cut PMN-PT substrate are given in **Figure S2** in the Supporting Information. Through the butterfly-like strain curve, we can see that the compressive strain can be as large as -0.5% under 8 kV cm^{-1} , which is a major factor in the E-field regulation.

Figure 3d is a summary of the M – H loops as a function of t_{Ru} and applied E-field, providing a qualitative analysis for the voltage tunable RKKY interaction. The red region represents single-loop mode with two CoFeB moments parallel to each other and the blue region represents the double mode, respectively. The relative color is a result of both the measured data and the estimations of AFM–FM coupling status. There are rich magnetic behaviors in this voltage tunable device, and the reversible single–double loop switching is a prototype for the potential GMR memories.

We further carried out spin dynamic measurement via FMR technique to quantitatively determine the anisotropy change of the E-field control process, as displayed in **Figure 4**. The SAF heterostructures with RKKY interaction enable dual mode FMR spectra and we can identify both acoustic mode (AM) and optical mode (OM) in the measured spectra. The following simplified FMR equations can be used to describe the AM and OM modes along the in-plane easy axis^[16,17]:

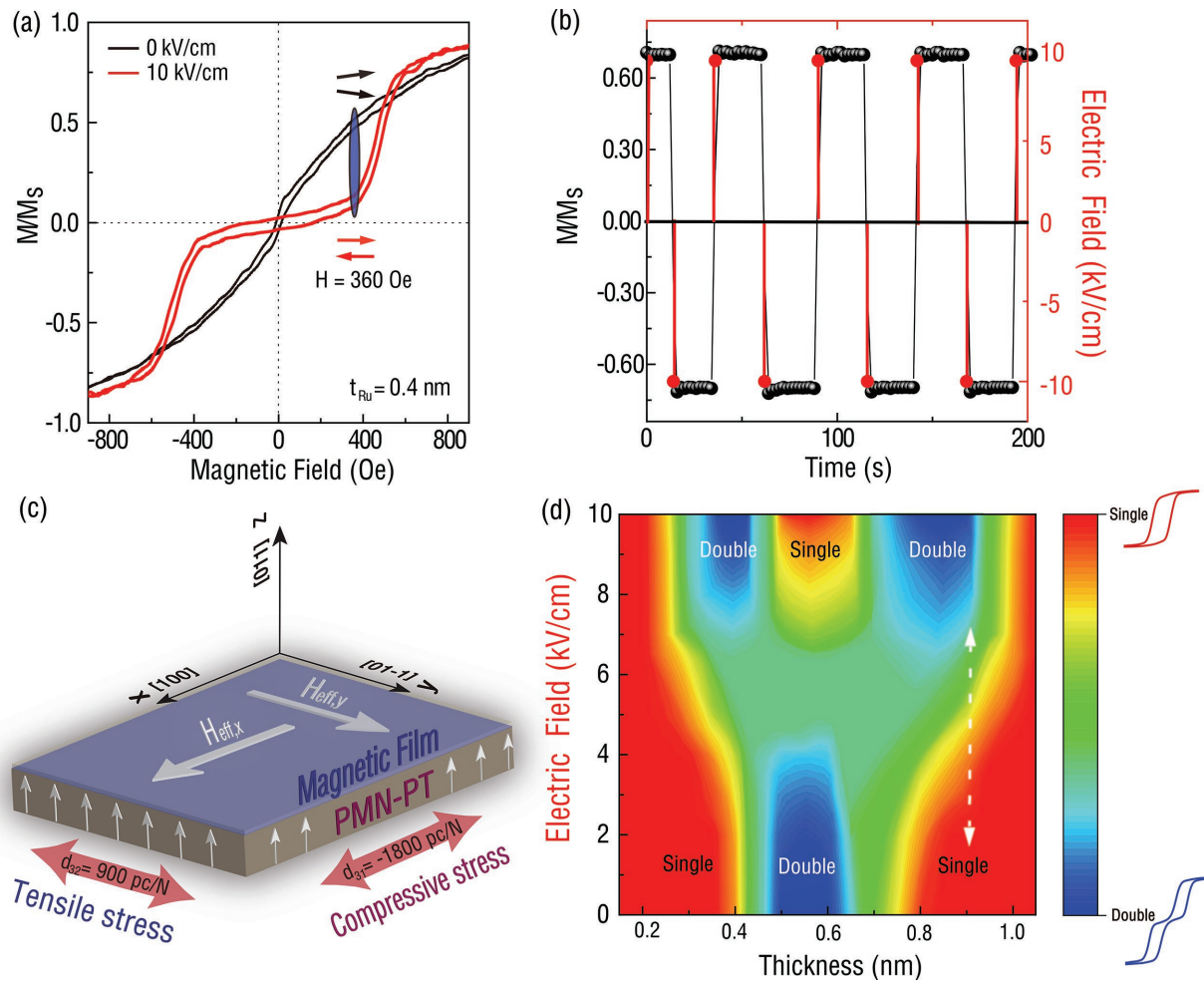


Figure 3. a) Magnetic hysteresis loops switching for the typical $t_{\text{Ru}} = 0.4$ nm SAF along [100] direction. b) Corresponding E-field-impulse-induced nonvolatile switching for the 0.4 nm sample with an assisted 360 Oe H-field. c) Stress condition analysis of PMN-PT piezoelectric substrate. d) The RKKY interaction phase diagram showing the double–single loop switching behavior with the variation of Ru thickness and external E-field.

$$\frac{f}{\gamma} = \sqrt{(H_r - H_k)(H_r + 4\pi M)} \quad (1)$$

$$\frac{f}{\gamma} = \sqrt{(H_r - H_k - J_{\text{RKKY}})(H_r - J_{\text{RKKY}} + 4\pi M)} \quad (2)$$

where f is the angular resonance frequency (9.76 GHz), γ is the gyromagnetic ratio of 2.8 MHz Oe^{-1} , H_r is the resonance field, H_k relates to the volume magnetocrystalline anisotropy, and $4\pi M$ is 13 kOe for FeCoB at room temperature.^[7] J_{RKKY} is the effective RKKY interaction field, which can be determined directly by the FMR field difference between AM and OM modes (calculated in Figure 5). A positive J_{RKKY} indicates an AFM coupling whereas a negative J_{RKKY} represents an FM coupling.^[16,17] Therefore, AM mode is higher than OM mode in FM coupling (0.4 nm) or lower than OM mode in AFM coupling (0.6 nm). Figure 4a,b displays the voltage control effect for both the 0.4 and 0.6 nm SAFs, where the upper pictures are the measured spectra under various E-field and the lower pictures are the corresponding phase diagrams with detailed information.

With an increasing bias voltage, the AM and OM modes in both SAFs are moving closer to each other, demonstrating the trend of AFM–FM coupling switching. The reason why AM and OM modes did not switch completely probably is that the FMR and VSM measurements have different principles and they provide different information for the voltage tunable RKKY interaction. The FMR is a perturbative method with only a small amount of magnetizations involved,^[18] while VSM reverses the whole magnetization. During the VSM measurement, the H-field sweep between positive and negative values, the inner magnetic dipole interaction and exchange interaction^[19] bring the encounter of energy barriers and make the magnetization reverse. This process can form a new domain, which will not happen in the FMR measurement. FMR happens only at a certain field, which satisfies the resonance condition; it is good at angular tests and can provide spatial anisotropy distribution with high precision. Figure 4c,d is the in-plane angular dependences of E-field-tuned AM/OM resonance field for the 0.4 and 0.6 nm SAFs. The applied voltage makes both OM and AM magnetic anisotropy rotate $\approx 90^\circ$, which is illustrated by the reversal of maximum and minimum H_r .

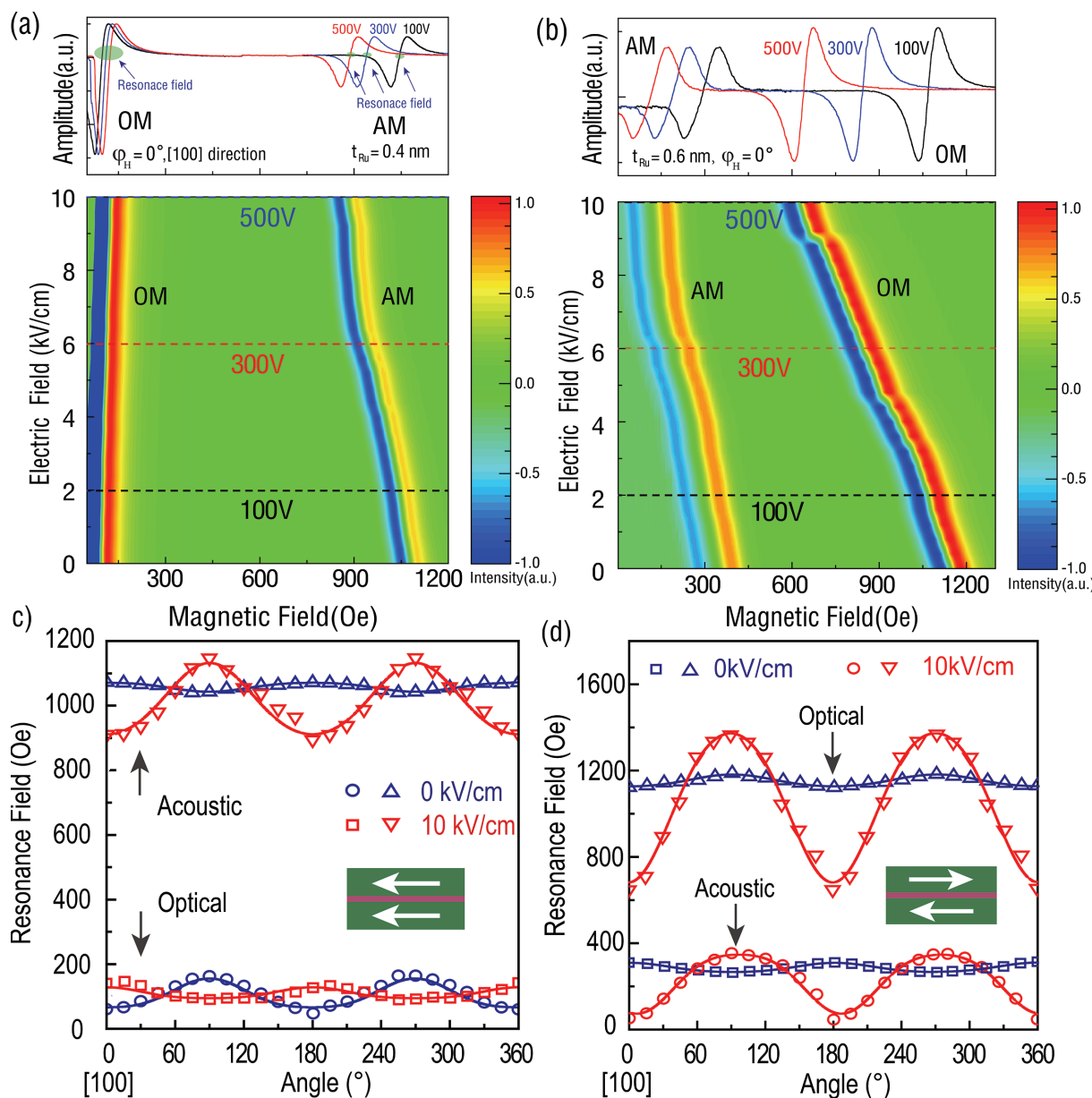


Figure 4. Spin dynamic measurements in E-field controllable SAFs. a,b) FMR spectra for the FM-coupled 0.4 nm SAF (a) and the AFM-coupled 0.6 nm SAF (b) while under various external E-fields. The upper pictures are the measured lines while the lower pictures are the detailed phase diagrams. The blue color represents the peak trough of the spectral line while the orange/yellow color is the wave peak of the resonance profile. c) FMR angular study of both AM and OM modes for the SAF with $t_{Ru} = 0.4$ nm. d) Angular dependence for the 0.6 nm AFM-coupled SAF; 0° is the [100] direction while 90° is the [01-1] direction.

The coupling coefficient can be quantitatively determined by the following equation:^[7,17]

$$J_{RKKY} = -\frac{2J_{inter}}{tM_s} \quad (3)$$

where t is the single FM layer thickness and J_{inter} is the coupling coefficient. According to the resonance fields of AM and OM modes, we can obtain the value of J_{RKKY} based on Equations (1) and (2), and then the value of J_{inter} . Take the [100] direction as an example ($\phi_H = 0^\circ$), we calculated J_{inter} as

a function of external E-field. As shown in **Figure 5**, with an increasing voltage, the exchange coupling constant J_{inter} of the FM-coupled 0.4 nm SAF decreases from 0.76 to 0.59 erg cm⁻², while J_{inter} of the 0.6 nm SAF changes from -0.62 to -0.40 erg cm⁻². This is accordant with the phenomenon that the FM/AFM coupling strength is reduced during the voltage control process.

To theoretically understand the strain effect on the IEC, a first-principles calculation with Green function method based on tight-binding linear muffin-tin orbital (TB-LMTO)^[20] is carried out to calculate the IEC of CoFe/Ru/CoFe trilayer as

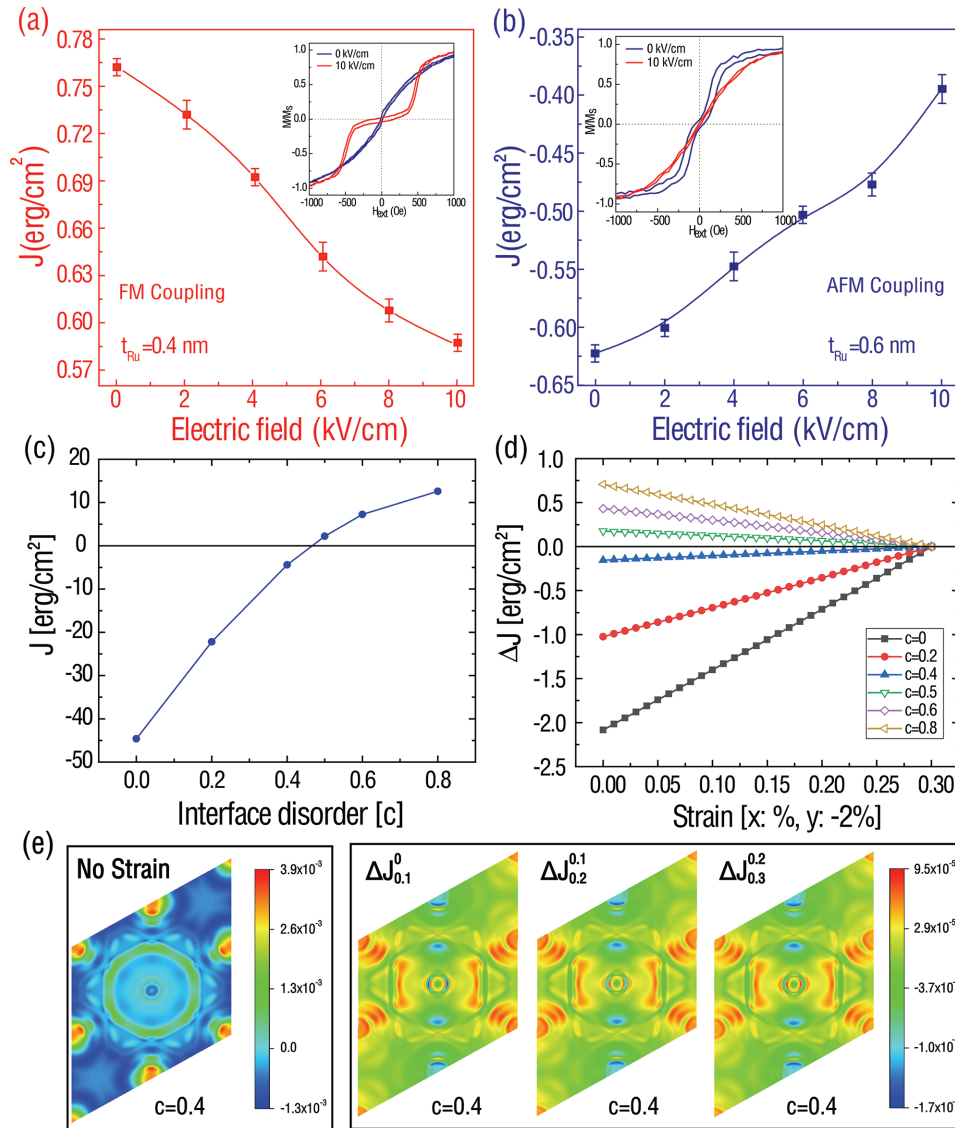


Figure 5. The variation of coupling coefficient under applied E-field. a) J_{inter} variation for the FM-coupled 0.4 nm SAF. b) Voltage dependence of J_{inter} for the AFM-coupled 0.6 nm SAF. J_{inter} is calculated based on the H_r of [100] direction, the inserted pictures are the corresponding hysteresis loops along [100] direction. c) Interface disorder dependence of J from first principles in Cu/CoFe (1.5 nm)/Ru (0.85 nm)/CoFe (1.5 nm)/Cu multilayers without any strain. The inset is the model of the calculation and also shows a sketch of the interface disorder ($[\text{CoFe}]_{1-x}\text{Ru}_x$). d) The influence of strain on J for different interface disorder case. For a better view of the tendency, we only plot the $\Delta J = J - J(\text{strain} = 0.3)$. It should be noted that strain means, for example, strain = 0.3, the system is stretched by 0.3% in the x-direction and compressed by 0.6% in the y-direction and a corresponding z to make the volume constant. e) The dimensionless k_{\parallel} -resolved J for typical strains from (d) with $c = 0.4$, and the $\Delta J_x^y = J_x - J_y$ with x and y represent the strains. It should be noted that, due to the strain the k_{\parallel} points will be shifted a little bit, and they are moved back to calculate the ΔJ_x^y for a clear view on the change of the RKKY.

$$J(\theta) = -\frac{1}{\pi} \text{Im} \int_{\Lambda} \int_{\mathcal{C}} f(z) \text{tr} \ln \left[1 - \frac{1 - \cos \theta}{2} M(k_{\parallel}, z) \right] dz \quad (4)$$

where θ is the angle between two CoFe layers, $f(z)$ is the Fermi-Dirac distribution for a complex energy z , Λ is the total lateral 2D Brillouin zone (BZ) area with sampled 20 000 k_{\parallel} inside to make sure the results converged in this work and $M(k_{\parallel}, z)$ can be further expanded as

$$M(k_{\parallel}, z) = - \left(1 - S_{RL}^{\alpha} \overline{\mathcal{G}}_L^{\uparrow} S_{LR}^{\alpha} \overline{\mathcal{G}}_R^{\uparrow} \right)^{-1} S_{RL}^{\alpha} \left(\overline{\mathcal{G}}_L^{\uparrow} - \overline{\mathcal{G}}_L^{\downarrow} \right) \left(1 - S_{LR}^{\alpha} \overline{\mathcal{G}}_R^{\downarrow} S_{RL}^{\alpha} \overline{\mathcal{G}}_L^{\downarrow} \right)^{-1} S_{LR}^{\alpha} \left(\overline{\mathcal{G}}_R^{\uparrow} - \overline{\mathcal{G}}_R^{\downarrow} \right) \quad (5)$$

The device is divided into the left (L) and right (R) subsystems by the middle of the Ru to use the surface Green function (SGF) technique, $S_{RL/LR}^{\alpha}$ denotes the coupling of the neighboring

principle layers between the left and right subsystems, and $\overline{G_{L/R}^\sigma}$ are the configurationally averaged SGF of the left/right part for the spin σ .^[21] To compute the averaged SGF, the coherent potential approximation (CPA)^[22] is applied in combination with the renormalization-decimation technique.^[23] We use $\theta = \pi$ for IEC calculations as the $J(\theta)$ reaches maximum value, while other values can be obtained analytically. All calculations are carried out in room temperature ($T = 300$ K) with the structures as shown in the inset of Figure 5c. Moreover, the IEC can vary from AFM coupling to FM coupling with interface disorders,^[12,20] so we first calculated the IEC as a function of interface disorder without any strain. The results are plotted in Figure 5c. Unsurprisingly, the IEC also crosses the zero axis.

Based on previous results, the strain is added by changing the lattice constant in our calculation under the rule of the PMN-PT piezoelectric substrate. However, it is obvious that the changing of PMN-PT will not affect the z -direction of CoFe/Ru/CoFe trilayer, so only the in-plane vectors (x, y) are strained with PMN-PT, and the out of plane vector (z) is then determined by keeping the volume constant. We can see the relation between the strain and the changing of IEC in Figure 5d, and the IEC strength (FM or AFM) all decays close to zero, which shows good agreement with the experimental results in Figure 5a,b for both FM and AFM case.

The origin of this phenomenon can be understood by the symmetry breakup as shown in Figure 5e, which is the dimensionless k_{\parallel} -resolved IEC in the lateral BZ for typical strains from Figure 5d with $c = 0.4$. In detail, without strain, the symmetry of k_{\parallel} -resolved IEC agrees with the C_{6v} symmetry of the in-plane lattice of CoFe (fcc [111] plane in our calculation). However, after changing the in-plane vector, the BZ is also slightly distorted, which ends up to a reconfiguration of the Fermi surface. This strain-mediated IEC modulation turns out to be a result of Fermi level tuning and has some consistency to our previous work.^[12,15] In this case, as represented in Figure 5e, with increasing the strain, the k_{\parallel} -resolved IEC break the C_{6v} symmetry, and found few region decrease (cold color), but more increase (warm color), which results that the integration of the k_{\parallel} -resolved IEC becomes larger and the AFM coupling fall weak.

In summary, voltage modulation of the RKKY exchange coupling in the SAFs has been demonstrated based on the FeCoB/Ru/FeCoB sandwich structures, in which we realized E-field controllable single–double M – H loop switching. The spin dynamic processes in the voltage tunable SAFs were studied by spatial FMR, which can give a quantitative understanding of the AFM–FM magnetic bi-state switching by the calculations of the effective RKKY coupling coefficient. Besides, we carried out the first-principles calculation to investigate the IEC in a relevant system and found that the reconfiguration of the Fermi surface is the reason related to this AFM–FM bilateral switching. This voltage regulation of RKKY interaction in a reversible and stable manner is a significant improvement for the E-field controllable AFM coupling and also paves a way for next generation of switchable AFM–FM spintronics.

Experimental Section

Sample Growth: Fe₆₀Co₂₀B₂₀ (15 nm)/Ru (x nm)/Fe₆₀Co₂₀B₂₀ (15 nm) trilayer heterostructures with various Ru thickness (x nm) were deposited

onto (011)-oriented PMN-PT substrates by DC magnetron sputtering at room temperature. Plasma etching was used to clean the surface. An in-plane H-field of ≈ 90 Oe was applied along [100] direction to form in-plane anisotropy. The background pressure was 2.0×10^{-7} Torr.

Magnetic Property Measurements: Voltage control of the SAFs investigations were carried out by applying voltages across the PMN-PT substrate thickness direction. The in situ E-field control of RKKY interaction was carried out based on VSM (Lake Shore 7404). FMR spectra were taken by Bruker EMX EPR spectrometer with a TE₁₀₂ cavity. The operated microwave field frequency was 9.76 GHz and the microwave power was 10 mW. For the angular-dependent FMR spectra measurements, in-plane angular rotation measurement was carried out by attaching the sample to a rotatable holder and started rotation from the [100] direction (defined as 0°; the [01–1] direction is 90°). All measurements were conducted at room temperature.

Supporting Information

Supporting Information is available from the Wiley Online Library or from the author.

Acknowledgements

X.W., Q.Y., and L.W. contributed equally to this work. This work was supported by the W. M. Keck Foundation and the NSF ERC Award 1160504, Z.Z. and M.L. were supported by the China Recruitment Program of Global Youth Experts and the Natural Science Foundation of China under Grants 51472199, 11534015, and 51602244. Q.Y. was supported by the Fundamental Research Funds for the Central Universities xjj2018207. L.W. and T.M. were supported by National Key Research Program of China 2016YFA0300702 and Shanxi Province Science and Technology Innovation Project 2015ZS-02.

Conflict of Interest

The authors declare no conflict of interest.

Keywords

antiferromagnetic spintronics, electric field control, magnetoelectric coupling, Ruderman–Kittel–Kasuya–Yosida interactions, synthetic antiferromagnetic multilayers

Received: June 7, 2018

Revised: July 11, 2018

Published online: August 22, 2018

- [1] a) P. Wadley, B. Howells, J. Železný, C. Andrews, V. Hills, R. P. Campion, V. Novák, K. Olejník, F. Maccherozzi, S. Dhesi, *Science* **2016**, *351*, 587; b) J. Železný, H. Gao, K. Výborný, J. Zemen, J. Mašek, A. Manchon, J. Wunderlich, J. Sinova, T. Jungwirth, *Phys. Rev. Lett.* **2014**, *113*, 157201.
- [2] B. Chen, H. Xu, C. Ma, S. Mattauch, D. Lan, F. Jin, Z. Guo, S. Wan, P. Chen, G. Gao, F. Chen, Y. Su, W. Wu, *Science* **2017**, *357*, 191.
- [3] a) J. Nishitani, K. Kozuki, T. Nagashima, M. Hangyo, *Appl. Phys. Lett.* **2010**, *96*, 221906; b) T. Kampfrath, A. Sell, G. Klatt, A. Pashkin, S. Mährlein, T. Dekorsy, M. Wolf, M. Fiebig, A. Leitenstorfer, R. Huber, *Nat. Photonics* **2011**, *5*, 31; c) Z. Jin, Z. Mics, G. Ma, Z. Cheng, M. Bonn, D. Turchinovich, *Phys. Rev. B* **2013**, *87*, 094422; d) J. Nishitani, T. Nagashima, M. Hangyo, *Phys. Rev. B* **2012**, *85*, 174439;

- e) M. Liu, Z. Zhou, T. Nan, B. M. Howe, G. J. Brown, N. X. Sun, *Adv. Mater.* **2013**, *25*, 1435; f) J. Lou, M. Liu, D. Reed, Y. Ren, N. X. Sun, *Adv. Mater.* **2009**, *21*, 4711.
- [4] a) W.-G. Wang, M. Li, S. Hageman, C. Chien, *Nat. Mater.* **2012**, *11*, 64; b) W. Wang, C. Chien, *J. Phys. D: Appl. Phys.* **2013**, *46*, 074004; c) S. Fukami, C. Zhang, S. DuttaGupta, A. Kurenkov, H. Ohno, *Nat. Mater.* **2016**, *15*, 535; d) J. C. Slonczewski, *J. Magn. Magn. Mater.* **1996**, *159*, L1; e) M.-H. Tsai, P.-H. Lin, K.-F. Huang, H.-H. Lin, C.-H. Lai, arXiv preprint arXiv:1706.01639 **2017**; f) A. MacDonald, M. Tsoi, *Philos. Trans. R. Soc., A* **2011**, *369*, 3098.
- [5] a) Q. Yang, Z. Zhou, N. Sun, M. Liu, *Phys. Lett. A* **2017**, *381*, 1213; b) M. Liu, J. Lou, S. Li, N. X. Sun, *Adv. Funct. Mater.* **2011**, *21*, 2593.
- [6] a) Y. Wang, X. Zhou, C. Song, Y. Yan, S. Zhou, G. Wang, C. Chen, F. Zeng, F. Pan, *Adv. Mater.* **2015**, *27*, 3196; b) V. Laukhin, V. Skumryev, X. Martí, D. Hrabovsky, F. Sánchez, M. García-Cuenca, C. Ferrater, M. Varela, U. Lüders, J.-F. Bobo, *Phys. Rev. Lett.* **2006**, *97*, 227201.
- [7] S. Li, Q. Li, J. Xu, S. Yan, G. X. Miao, S. Kang, Y. Dai, J. Jiao, Y. Lü, *Adv. Funct. Mater.* **2016**, *26*, 3738.
- [8] X. Liu, S. Ishio, H. Ma, *J. Nanomater.* **2015**, *2015*, 5.
- [9] S. Li, C. Wang, X.-M. Chu, G.-X. Miao, Q. Xue, W. Zou, M. Liu, J. Xu, Q. Li, Y. Dai, *Sci. Rep.* **2016**, *6*, 33349.
- [10] P. Bruno, C. Chappert, *Phys. Rev. Lett.* **1991**, *67*, 1602.
- [11] C.-W. Cheng, T.-I. Cheng, C. Shiue, C.-L. Weng, Y.-C. Tsai, G. Chern, *IEEE Trans. Magn.* **2013**, *49*, 4433.
- [12] Q. Yang, L. Wang, Z. Zhou, L. Wang, Y. Zhang, S. Zhao, G. Dong, Y. Cheng, T. Min, Z. Hu, W. Chen, K. Xia, M. Liu, *Nat. Commun.* **2018**, *9*, 991.
- [13] J.-C. A. Huang, C. Hsu, S. Chen, C. Liu, Y. Liao, M. Lin, C. Lee, *J. Appl. Phys.* **2007**, *101*, 123923.
- [14] a) S. Byeon, A. Misra, W. Doyle, *IEEE Trans. Magn.* **2004**, *40*, 2386; b) P. Bruno, C. Chappert, *Phys. Rev. B* **1992**, *46*, 261; c) K. Kim, S. Jang, K. Shin, H. Kim, T. Kang, *J. Appl. Phys.* **2001**, *89*, 7612.
- [15] Q. Yang, Z. Zhou, L. Wang, H. Zhang, Y. Cheng, Z. Hu, B. Peng, M. Liu, *Adv. Mater.* **2018**, *30*, 1800449.
- [16] Y. Gong, Z. Cevher, M. Ebrahim, J. Lou, C. Pettiford, N. Sun, Y. Ren, *J. Appl. Phys.* **2009**, *106*, 063916.
- [17] X. Xing, M. Liu, S. Li, O. Obi, J. Lou, Z. Zhou, B. Chen, N. Sun, *IEEE Trans. Magn.* **2011**, *47*, 3104.
- [18] a) H. Xi, R. M. White, S. M. Rezende, *Phys. Rev. B* **1999**, *60*, 14837; b) V. I. Nikitenko, V. S. Gornakov, L. M. Dedukh, Y. P. Kabanov, A. F. Khapikov, A. J. Shapiro, R. D. Shull, A. Chaiken, R. P. Michel, *Phys. Rev. B* **1998**, *57*, R8111.
- [19] a) D. C. Johnston, *Phys. Rev. B* **2016**, *93*, 014421; b) J. B. Staunton, B. L. Gyorffy, J. Poulter, P. Strange, *J. Phys. C: Solid State Phys.* **1988**, *21*, 1595.
- [20] S. Wang, K. Xia, T. Min, Y. Ke, *Phys. Rev. B* **2017**, *96*, 024443.
- [21] I. Turek, V. Drchal, J. Kudrnovský, M. Šob, P. Weinberger, *Electronic Structure of Disordered Alloys, Surfaces and Interfaces*, Springer Science+Business Media, New York **1997**.
- [22] a) B. Velický, S. Kirkpatrick, H. Ehrenreich, *Phys. Rev.* **1968**, *175*, 747; b) P. Soven, *Phys. Rev.* **1967**, *156*, 809; c) B. Velický, *Phys. Rev.* **1969**, *184*, 614.
- [23] M. L. Sancho, J. L. Sancho, J. M. L. Sancho, J. Rubio, *J. Phys. F: Met. Phys.* **1985**, *15*, 851.